Themed Issue: Drug Addiction - From Basic Research to Therapies
Guest Editors - Rao Rapaka and Wolfgang Sadée

N-n-Alkylnicotinium Analogs, a Novel Class of Antagonists at α4β2* Nicotinic Acetylcholine Receptors: Inhibition of S(-)-Nicotine-Evoked 86Rb+ Efflux from Rat Thalamic Synaptosomes

Submitted: August 18, 2005; Accepted: September 12, 2005; Published: January 13, 2006

Lincoln H. Wilkins Jr,[1,2] Dennis K. Miller,[3] Joshua T. Ayers,[4] Peter A. Crooks,[1] and Linda P. Dwoskin[1]

[1]College of Pharmacy, University of Kentucky, Lexington, KY 40536-0082
[2]Current address: Bristol-Myers Squibb Co, 309 Dove Park Road, Covington, LA 70433
[3]Department of Psychological Services, 208 McAlester Hall, University of Missouri, Columbia, MO 65211
[4]AstraZeneca, 1800 Concord Pike, PO Box 15437, Wilmington, DE 19850-5437

ABSTRACT

Pyridine *N*-*n*-alkylation of S(-)-nicotine (NIC) affords *N*-*n*-alkylnicotinium analogs, previously shown to competitively inhibit [^{3}H]NIC binding and interact with α4β2* nicotinic receptors (nAChRs). The present study determined the ability of the analogs to inhibit NIC-evoked $^{86}Rb^+$ efflux from rat thalamic synaptosomes to assess functional interaction with α4β2* nAChRs. In a concentration-dependent manner, NIC evoked $^{86}Rb^+$ efflux (EC_{50} = 170 nmol/L). Analog-induced inhibition of NIC-evoked $^{86}Rb^+$ efflux varied over a ~450-fold range. Analogs with long *n*-alkyl chain lengths (C_9-C_{12}) inhibited efflux in the low nmol/L range (IC_{50} = 9-20 nmol/L), similar to dihydro-β-erythroidine (IC_{50} = 19 nmol/L). Compounds with shorter *n*-alkyl chain lengths (C_1-C_8) produced inhibition in the low μmol/L range (IC_{50} = 3-12 μmol/L). C_{10} and C_{12} analogs completely inhibited NIC-evoked efflux, whereas $C_{1\text{-}9}$ analogs produced maximal inhibition of only 10% to 60%. While the C_{10} analog *N*-*n*-decylnicotinium iodide (NDNI) did not produce significant inhibition of NIC-evoked dopamine release in previously reported studies, NDNI possesses high affinity for [^{3}H]NIC binding sites (K_i = 90 nmol/L) and is a potent and efficacious inhibitor of NIC-evoked $^{86}Rb^+$ efflux as demonstrated in the current studies. Thus, NDNI is a competitive, selective antagonist at α4β2* nAChRs.

KEYWORDS: nicotine analogs, subtype-selectivity, neuronal nicotinic receptor

INTRODUCTION

Activation of neuronal nicotinic receptors (nAChR) results in the transient opening of its ligand-gated ion channel, permitting Ca^{2+}, Na^+, and K^+ flux, followed by local depolarization of the plasma membrane.[1] The α4β2* nAChR is the predominant heteromeric nAChR subtype in brain, and high affinity S-(-)-[^{3}H]nicotine ([^{3}H]NIC) binding to rodent brain membranes has been used to probe the interaction of various ligands with this site. Of importance, high affinity [^{3}H]NIC binding sites are immunoprecipitated with anti-β2 and anti-α4 antibodies,[2-4] and mice lacking the β2 subunit do not exhibit high affinity [^{3}H]NIC binding[5,6] and demonstrate essentially eliminated dihydro-β-erythroidine-sensitive and -resistant $^{86}Rb^+$ efflux from thalamus and cerebral cortex.[7,8] The $^{86}Rb^+$ efflux assay monitors K^+ flux through nAChR channels and characterizes functional interactions with the high affinity [^{3}H]NIC binding site in native brain tissue preparations (ie, α4β2* nAChRs[7,9-11]) and in cell lines.[12,13] $^{86}Rb^+$ efflux is used also to measure the function of other nAChR receptor subtypes when various subunit combinations are expressed in cell lines.[14-18]

Nicotinic agonist potency in the $^{86}Rb^+$ efflux assay using native rodent preparations is highly correlated with affinity for [^{3}H]NIC binding sites, but not with affinity for α-[^{125}I]bungarotoxin binding.[9] Surprisingly, inhibition of NIC-evoked $^{86}Rb^+$ efflux by a small number of nAChR antagonists was not correlated with affinity for [^{3}H]NIC binding sites.[9] However, only a limited number of structurally-unrelated nAChR antagonists were investigated in the latter study, likely precluding the establishment of a structure-activity relationship.

Pyridine *N*-*n*-alkylation of NIC has afforded a series of *N*-*n*-alkylnicotinium analogs with carbon chains of C_1-C_{12}.[19-23] As a result of *N*-*n*-alkylation, NIC is converted from a potent agonist into a series of novel compounds with potent and subtype-selective nAChR antagonist properties. The C_8 analog *N*-*n*-octylnicotinium iodide (NONI) has been identified as a potent selective inhibitor of nAChR subtypes mediating NIC-evoked [^{3}H]dopamine ([^{3}H]DA) overflow from superfused rat striatal slices.[22] NONI almost completely inhibited NIC-evoked [^{3}H]DA overflow (Imax = 90%). Of importance, NONI did not exhibit high affinity for [^{3}H]NIC

Corresponding Author: Linda P. Dwoskin, College of Pharmacy, University of Kentucky, Lexington, KY 40536-0082. Tel: (859) 257-4743; Fax: (859) 257-7564; E-mail: ldwoskin@email.uky.edu

binding sites, indicative of nAChR subtype selectivity.[23] In contrast, the C_{10} analog *N*-*n*-decylnicotinium iodide (NDNI) exhibited high affinity for [^{3}H]NIC binding sites but did not inhibit NIC-evoked [^{3}H]DA overflow, again indicative of nAChR subtype selectivity.[22,23] In both [^{3}H]DA release and [^{3}H]NIC binding assays, inhibitory potency of the analog series was correlated with *n*-alkyl chain length (ie, potency increased with increasing *n*-alkyl chain length). Thus, these results indicate that NDNI selectively interacts with the α4β2* nAChR subtype, that NONI is a selective antagonist at nAChR subtypes mediating NIC-evoked DA release, and that nAChR subtypes primarily mediating NIC-evoked DA release from rat striatal slices is not of α4β2* composition.

Inhibition of [^{3}H]NIC binding does not determine whether these *N*-*n*-alkylnicotinium analogs act as nAChR agonists or antagonists at high affinity [^{3}H]NIC binding sites. The purpose of the current study was to evaluate the functional interaction of this series of *N*-*n*-alkylnicotinium analogs at the α4β2* nAChR subtype using $^{86}Rb^+$ efflux from rat striatal synaptosomes. Initially, the time- and concentration-dependence of the response to NIC in the $^{86}Rb^+$ efflux assay was investigated. Subsequently, analog-induced $^{86}Rb^+$ efflux (intrinsic activity, agonist response) and ability to inhibit NIC-evoked $^{86}Rb^+$ efflux (antagonist activity) were determined and compared with that produced by dihydro-β-erythroidine (DHβE), a classical competitive nAChR antagonist.

MATERIALS AND METHODS

NIC, DHβE, and *N*-[2-hydroxyethyl]-piperizine-*N*'-[2-ethanesulfonic acid] (HEPES) were purchased from Sigma/RBI (Natick, MA). α-D-Glucose was purchased from Aldrich Chemical Co (Milwaukee, WI). ^{86}Rubidium chloride (initial specific activity ~100-400 Ci/moL) was obtained from PerkinElmer Life Sciences (Boston, MA). The remaining chemicals contained in the superfusion buffer were obtained from Fisher Scientific (Pittsburgh, PA). *N*-Methylnicotinium iodide (NMNI), *N*-*n*-propylnicotinium iodide (NPNI), *N*-*n*-butylnicotinium iodide (NnBNI), and NONI were prepared as described by Crooks et al.[19] *N*-Ethylnicotinium iodide (NENI), *N*-*n*-hexylnicotinium iodide (NHxNI), *N*-*n*-heptylnicotinium iodide (NHpNI), *N*-*n*-nonylnicotinium iodide (NNNI), NDNI, and *N*-*n*-dodecylnicotinium iodide (NDDNI) were prepared from NIC and the appropriate *n*-alkyl iodide using the general procedure described by Xu et al.[24] All synthesized compounds were fully characterized by elemental analysis and determined to be free from NIC using spectroscopic (^{1}H- and ^{13}C-nuclear magnetic resonance, and fast atom bombardment mass spectroscopy), thin layer chromatographic (silica gel), and combustion analysis procedures. Structures of the *N*-*n*-alkylnicotinium analogs are provided in Figure 1.

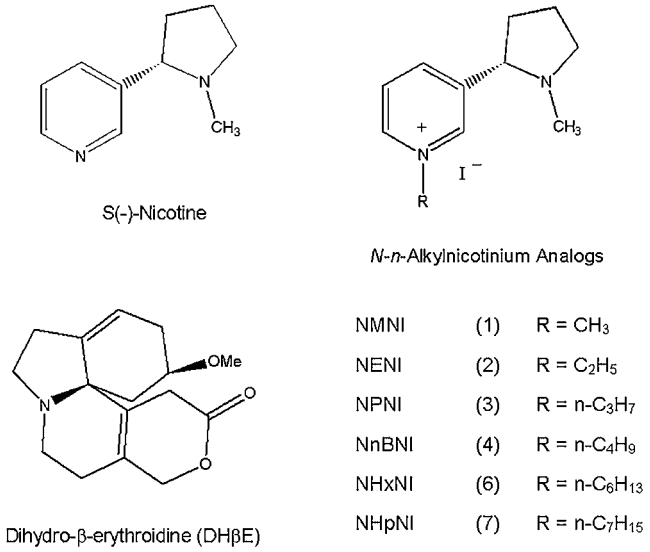

Figure 1. Structures of NIC, *N*-*n*-alkylnicotinium analogs and DHβE. The carbon number in parentheses to the right of each analog acronym indicates the number of carbons in the respective *n*-alkyl substituent. Note that the 2' *S* configuration of the nicotine molecule is preserved in each of the *N*-*n*-alkylnicotinium analogs.

Male Sprague-Dawley rats (200-250 g) were obtained from Harlan Laboratories (Indianapolis, IN) and were housed 2 per cage with free access to food and water in the Division of Laboratory Animal Resources at the College of Pharmacy, University of Kentucky. Experimental protocols involving animals were in accordance with the 1996 National Institutes of Health (NIH) Guide for the Care and Use of Laboratory Animals and were approved by the Institutional Animal Care and Use Committee at the University of Kentucky. For each experiment, thalamus from an individual rat was dissected and gently homogenized (20 up and down strokes of a Teflon-glass homogenizer) in 1 mL ice-cold buffer (320 mM sucrose and 5 mM HEPES, pH 7.5). Subsequently, homogenate was centrifuged (3000*g* for 10 minutes at 4°C) using a Beckman centrifuge (model GS-15R, Beckman Coulter, Fullerton, CA), and the supernatant was centrifuged (12 000*g* for 20 minutes at 4°C). The resulting pellet was resuspended in a volume of uptake buffer (140 mM NaCl, 1.5 mM KCl, 2 mM $CaCl_2$, 1 mM $MgSO_4$, 25 mM HEPES, 20 mM glucose; pH 7.5) providing a protein concentration of ~40 μg/25 μL synaptosomal suspension. Thalamic synaptosomes were used owing to the relatively high density of α4β2* nAChRs in this tissue.[10]

Synaptosomal aliquots (25 μL) were incubated with 10 μL of ^{86}RbCl (~0.5 mM total $^{86}Rb^+$ concentration) in uptake buffer for 30 minutes at ~25°C. $^{86}Rb^+$ uptake was terminated by filtration onto 6-mm diameter type gas chromatography (GC) glass fiber filters (Micro Filtration Systems, Dublin, CA) under gentle vacuum (~0.2 atm), followed by 3 washes with 0.5 mL uptake buffer at 25°C. The 6-mm

diameter glass fiber filters containing the $^{86}Rb^+$-preloaded synaptosomes were placed on 13-mm glass fiber filters (type A/E) positioned on plastic Swinney holders (Gelman Life Sciences Inc, Ann Arbor, MI) that were mounted on a polypropylene platform to begin superfusion. Synaptosomes were superfused (1.0 mL/min) with buffer containing 135 mM NaCl, 1.5 mM KCl, 2 mM $CaCl_2$, 1 mM $MgSO_4$, 5 mM CsCl, 50 nmol/L tetrodotoxin (TTX), 25 mM HEPES, 20 mM α-D-glucose, 1.0 g/L bovine serum albumin (BSA) (pH 7.5, ~25°C). CsCl and TTX were included in the buffer to block voltage-gated K^+ and Na^+ channels, respectively, and to reduce the rate of basal fractional $^{86}Rb^+$ outflow, thereby optimizing the signal-to-noise ratio.

To identify the concentration of NIC to be used in experiments determining *N*-*n*-alkylnicotinium analog-induced inhibition of NIC-evoked response, an initial series of experiments was performed in which the concentration-dependence of NIC to evoke $^{86}Rb^+$ efflux from preloaded thalamic synaptosomes was determined. Sample collection began after 8 minutes of superfusion. Superfusate fractions were collected in 20-second intervals (0.3 mL vol) into 4-mL scintillation vials using a Retriever II fraction collector (ISCO Inc, Lexana, KS). To determine the basal fractional $^{86}Rb^+$ outflow, samples were collected for a 5-minute period. After collection of 15 basal samples, synaptosomes from an individual rat were superfused in the absence or presence of 1 of 6 concentrations of NIC (30 nmol/L to 10 μmol/L) for 3 minutes to determine the concentration dependence of NIC-evoked $^{86}Rb^+$ efflux. Superfusion continued for an additional 3-minute period with buffer in the absence of NIC. Radioactivity in superfusate and tissue samples was determined by adding 3.7 mL water to each sample, followed by measurement of Cerenkov radiation using a scintillation counter (model B1600 TR, Packard Bioscience Co, Meriden, CT).

The ability of *N*-*n*-alkylnicotinium analogs (1 nmol/L to 100 μmol/L) to evoke $^{86}Rb^+$ efflux and to inhibit NIC-evoked $^{86}Rb^+$ efflux was determined and compared with DHβE (1 nmol/L to 100 μmol/L). Sample collection began after 8 minutes of superfusion. To determine basal fractional $^{86}Rb^+$ outflow, samples were collected for a 2-minute period. After collection of 6 basal samples, synaptosomes from an individual rat were superfused in the absence or presence of 1 of 6 concentrations of analog or DHβE for 3 minutes, to determine the intrinsic activity of the compounds to evoke $^{86}Rb^+$ efflux. Subsequently, NIC (1 μmol/L) was added to buffer and superfusion was continued for an additional 3 minutes, followed by superfusion for 3 minutes with buffer in the absence of analog or NIC. To maximize the ability to detect analog-induced inhibition of NIC-evoked $^{86}Rb^+$ efflux, the concentration (1 μmol/L) of NIC chosen for these experiments was at the top of the linear portion of the NIC concentration-response curve. Each aliquot of thalamic synaptosomes from an individual rat was exposed to only one concentration of analog or DHβE. In each experiment, one synaptosomal aliquot was exposed to NIC (1 μmol/L) in the absence of analog or DHβE (NIC control), and one synaptosomal aliquot was superfused in the absence of either NIC or analog (buffer control) to determine basal $^{86}Rb^+$ efflux during the entire course of the experiment. Thus, a repeated-measures design was used; the concentration response for analog-induced intrinsic and inhibitory activity was determined using synaptosomes from each rat.

To determine the baseline cpm for fractional $^{86}Rb^+$ outflow across the entire superfusion period, an exponential decay curve was fit to the data (cpm) preceding drug exposure and during the recovery period (Sigma Plot 2000, SPSS Inc, Chicago, IL). Subsequently, time-course data for analog-, DHβE-, and NIC-evoked increases in $^{86}Rb^+$ efflux were converted to fractional $^{86}Rb^+$ efflux by the equation (sample cpm – baseline cpm) ÷ baseline cpm. Fractional increases in $^{86}Rb^+$ efflux were summed to obtain total $^{86}Rb^+$ efflux during the entire period of superfusion with respective compound. To reduce variability within and between experiments, total $^{86}Rb^+$ efflux was normalized to $^{86}Rb^+$ content in the corresponding synaptosomal aliquot and then multiplied by 100, to obtain total $^{86}Rb^+$ efflux as a percentage of tissue $^{86}Rb^+$ content.

The initial series of experiments determining the concentration-dependence of NIC to increase fractional $^{86}Rb^+$ efflux was analyzed by analysis of variance (ANOVA), and the concentration-response curves were modeled to obtain pharmacological parameters. The time course of the concentration-dependent effect of NIC to increase fractional $^{86}Rb^+$ efflux from thalamic synaptosomes was analyzed also by 2-way repeated measures ANOVA with NIC concentration and collection fraction as within-subject factors. Subsequently, Dunnett's post hoc analyses determined the concentrations of NIC that increased fractional $^{86}Rb^+$ efflux above the mean basal $^{86}Rb^+$ outflow at specific collection fractions. Furthermore, the maximal increase in fractional $^{86}Rb^+$ efflux at each concentration of NIC was analyzed by 1-way ANOVA. Dunnett's analysis was used to determine significant differences between maximal NIC-evoked outflow and maximal fractional outflow in the buffer control condition. Tukey's test was used to determine differences in maximal effect produced by the various concentrations of NIC. NIC-evoked total $^{86}Rb^+$ efflux from thalamic synaptosomes was expressed as a function of log NIC concentration. Variable slope sigmoid concentration-response curves were fit to data using nonlinear least squares regression. The sigmoid curve was defined by the equation $Y = Bt + [(Tp - Bt)/(1 + 10^{(\log EC_{50} - X) \cdot n})]$, where Y is the total $^{86}Rb^+$ efflux expressed as percentage tissue content; X is the log NIC concentration; log EC_{50} is the log NIC concentration that increased $^{86}Rb^+$ efflux by 50%; n is the Hill coefficient; and

Bt and *Tp* are the minimum and maximum total $^{86}Rb^+$ efflux, respectively (*Bt* and *Tp* were allowed to vary to obtain a unique curve fit).

To determine the ability of the *N*-*n*-alkylnicotinium analogs to evoke total $^{86}Rb^+$ efflux (intrinsic activity) and to begin to assess structure-activity relationships, a 2-way ANOVA was performed with *n*-alkyl chain length as a between-groups factor and analog concentration as a within-subject factor. Subsequently, 1-way ANOVAs were performed for each analog and for DHβE to determine concentrations that significantly increased total $^{86}Rb^+$ efflux. Dunnett's post hoc analyses determined analog or DHβE concentrations increasing total $^{86}Rb^+$ efflux relative to buffer control.

To determine the ability of the *N*-*n*-alkylnicotinium analogs to inhibit NIC-evoked total $^{86}Rb^+$ efflux, data were expressed as NIC-evoked $^{86}Rb^+$ efflux as a function of the logarithm of analog concentration. Concentration-response curves were modeled using a variable slope sigmoid fit to the data. Inhibition curves were fit using nonlinear least squares regression, using the equation $Y = Bt + [(Tp - Bt)/(1 + 10^{(\log IC_{50} - X) \cdot n})]$, where *Y* is the total $^{86}Rb^+$ efflux expressed as percentage tissue content; *X* is the log NIC concentration; log IC_{50} is the log analog or DHβE concentration, which decreased $^{86}Rb^+$ efflux by 50%; *n* is the pseudo-Hill coefficient; and *Bt* and *Tp* are the minimum and maximum total $^{86}Rb^+$ efflux, respectively. All data parameters were derived from computer-aided curve fitting, and statistical analyses were performed using the commercially available software packages SigmaPlot (Version 6.0, Jandel Scientific, Corte Madera, CA), PRISM (Version 3.0, GraphPad Software Inc, San Diego, CA), and SPSS standard (Version 9.0, SPSS Inc, Chicago, IL). The SigmaPlot program used embedded macros for nonlinear regression fitting of efflux data (cpm). Unless noted otherwise, the best-fit curve was defined as that which minimized the absolute squared distance (Y^2) from each data point to the curve.

RESULTS

NIC-evoked $^{86}Rb^+$ Efflux

The time course of the concentration-response for NIC to evoke fractional $^{86}Rb^+$ efflux from $^{86}Rb^+$ preloaded rat thalamic synaptosomes is illustrated in Figure 2. Fractional $^{86}Rb^+$ efflux from thalamic synaptosomes was stable during the 440-second superfusion period with buffer alone (collection samples 1-22, Figure 2, top panel). Two-way repeated measures ANOVA of basal efflux prior to NIC exposure revealed that both the main effects and the chamber x superfusate sample interaction were not significant ($P > .05$). Maximal efflux in response to each NIC concentration (30 nmol/L to 10 μmol/L) was observed within the first or second 20-second superfusate sample. Response diminished thereafter, reaching levels of control efflux after 100 to 200 seconds, depending upon the NIC concentration. For subsequent analysis of the concentration-effect of NIC, data from collection samples 19 to 36 were analyzed by 2-way repeated measures ANOVA. A significant interaction of NIC

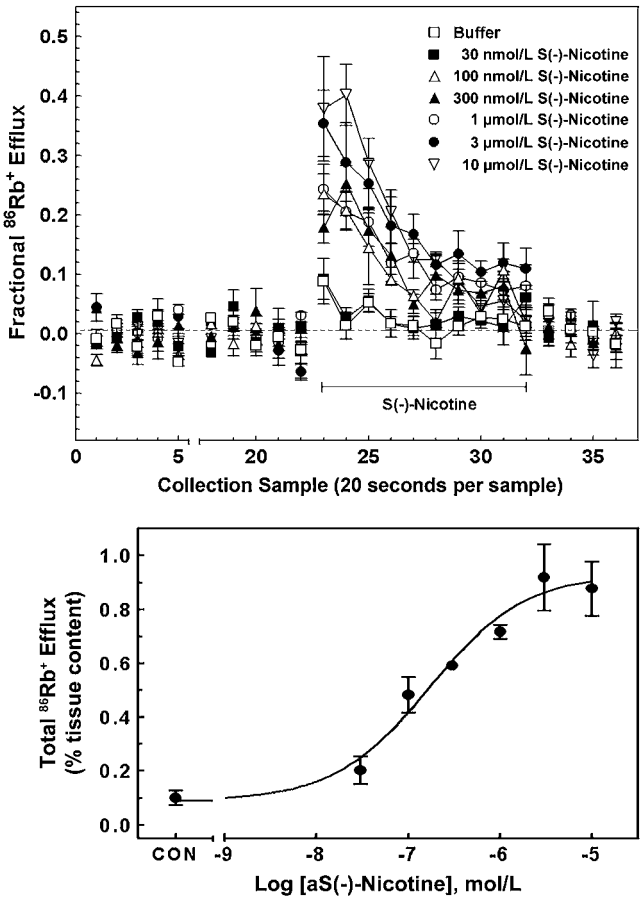

Figure 2. Time course and concentration response for NIC-evoked fractional $^{86}Rb^+$ efflux from preloaded rat thalamic synaptosomes. Top panel: Data are expressed as a fraction of basal $^{86}Rb^+$ outflow ([sample cpm – basal cpm]/basal cpm) in the absence and presence of NIC as a function of collection sample (20 seconds/sample). After collection of sample No. 22, superfusion buffer was changed to either buffer containing 1 of 6 concentrations (30 nmol/L – 10 μmol/L) of NIC or to control buffer (in the absence of NIC), and superfusion continued for 200 seconds. Legend indicates treatment condition; buffer indicates absence of NIC. Horizontal bar indicates duration of superfusion with NIC. Each data point represents the mean 6 SEM of 3 to 6 independent observations from individual rats. Bottom panel: Synaptosomes were superfused with buffer in the absence or presence of 6 concentrations of NIC for a 200-second period. Data are presented as total $^{86}Rb^+$ efflux as the area under the time-response curve (sum of cpm above baseline during NIC exposure ÷ tissue cpm) illustrated in Figure 2 (top panel). Tissue $^{86}Rb^+$ content (cpm) was determined at the end of the collection period. $^{86}Rb^+$ efflux from synaptosomes exposed to buffer (in the absence of NIC) constituted the control (CON) condition in each experiment. Each data point represents the mean 6 SEM of 4 to 6 independent observations.

concentration x collection sample was found ($F_{102,510}$ = 6.16; $P < .0001$). Of note, when the superfusion buffer was changed, a small but significant increase in $^{86}Rb^+$ efflux was observed in the chamber superfused with buffer only, which was likely due to mechanical manipulation of the system. Moreover, data from the first sample immediately following exposure to the various concentrations of NIC showed that fractional $^{86}Rb^+$ efflux increased in a concentration-dependent manner. A significant effect of NIC concentration on maximal $^{86}Rb^+$ efflux was found ($F_{6,41}$ = 14.1; $P < .0001$). Post hoc analysis revealed that the lowest NIC concentration (30 nmol/L) did not increase $^{86}Rb^+$ efflux compared with control, whereas higher concentrations of NIC increased the response. A plateau in the NIC concentration response was observed with 3 μmol/L; and 1 μmol/L NIC produced a reliable increase in fractional $^{86}Rb^+$ efflux across the duration of drug exposure.

Analysis of NIC-evoked total $^{86}Rb^+$ efflux from thalamic synaptosomes cumulated across the duration of superfusion with NIC revealed a sigmoid concentration-response curve (Hill coefficient = 0.84 ± 0.28, n_H ± SE; Figure 2, bottom panel). Maximal response was observed at 3 μmol/L, which resulted in 0.93% ± 0.08% SE of tissue $^{86}Rb^+$ content collected in superfusate during the 200-second period of exposure. The EC_{50} value for NIC to evoke total $^{86}Rb^+$ efflux was 170 nmol/L (95% confidence interval [CI], 43 nmol/L, 690 nmol/L). NIC at a concentration of 1 μmol/L produced a reliable response just below the maximum of the concentration-response curve. Thus, 1 μmol/L NIC was chosen to study *N*-*n*-alkylnicotinium analog inhibition in subsequent experiments.

N-n-Alkylnicotinium Analog-evoked Total $^{86}Rb^+$ Efflux

The ability of *N*-*n*-alkylnicotinium analogs to evoke total $^{86}Rb^+$ efflux from thalamic synaptosomes (intrinsic activity) was determined by cumulating the amount of $^{86}Rb^+$ efflux during the 200-second exposure to each concentration of analog to the superfusion buffer (Table 1). At the highest concentration (100 μmol/L) examined, NDNI (C_{10} analog) and NDDNI (C_{12} analog) evoked significant $^{86}Rb^+$ efflux, which did not return to basal levels, precluding calculation of total $^{86}Rb^+$ efflux (data not included in Table 1). Repeated-measures, 2-way ANOVA revealed a significant compound x concentration interaction ($F_{48,96}$ = 1.72; $P < .05$). Separate 1-way repeated-measures ANOVAs for each *N*-*n*-alkylnicotinium analog and for DHβE were performed. A significant main effect of concentration was found for NMNI (C_1: $F_{6,30}$ = 4.78; $P < .005$), NENI (C_2: $F_{6,32}$ = 3.74; $P < .01$), NnBNI (C_4: $F_{6,32}$ = 3.84; $P < .01$), NHxNI (C_6: $F_{6,31}$ = 3.55; $P < .05$), NNNI (C_9: $F_{6,34}$ = 4.01; $P < .01$), NDNI (C_{10}: $F_{6,34}$ = 2.68; $P < .05$), and DHβE ($F_{6,30}$ = 7.89; $P < .0001$); however, orderly concentration-dependent relationships were not observed.

N-n-Alkylnicotinium Analog-induced Inhibition of NIC-evoked $^{86}Rb^+$ Efflux

For each experiment assessing analog-induced inhibition of NIC (1 μmol/L) response, one synaptosomal aliquot served as a within-subject NIC control. The IC_{50} values were either in the nmol/L or in the μmol/L range (ie, a 3-order of magnitude difference in inhibition potency was observed).

Table 1. Intrinsic Activity Produced by the *N*-*n*-alkylnicotinium Analogs and DHβE in the $^{86}Rb^+$ Efflux Assay*

Compound	*n*-Alkyl Chain Length	Control	0.001 μmol/L	0.01 μmol/L	0.1 μmol/L	1 μmol/L	10 μmol/L	100 μmol/L
NMNI	1	0.08 ± 0.02	0.08 ± 0.02	0.15 ± 0.04	0.06 ± 0.01	0.01 ± 0.01	0.02 ± 0.01	0.04 ± 0.02
NENI	2	0.09 ± 0.01	0.41 ± 0.03	0.13 ± 0.06	0.10 ± 0.06	0.12 ± 0.04	0.10 ± 0.05	0.16 ± 0.08
NPNI	3	0.10 ± 0.02	0.10 ± 0.02	0.12 ± 0.06	0.03 ± 0.03	0.24 ± 0.10	0.08 ± 0.03	0.25 ± 0.09
NnBNI	4	0.12 ± 0.04	0.05 ± 0.03	0.01 ± 0.01	0.03 ± 0.02	0.00 ± 0.00	0.00 ± 0.00	0.00 ± 0.00
NHxNI	6	0.24 ± 0.06	0.09 ± 0.04	0.17 ± 0.07	0.04 ± 0.03	0.04 ± 0.03	0.02 ± 0.02	0.10 ± 0.02
NHpNI	7	0.07 ± 0.04	0.20 ± 0.09	0.11 ± 0.03	0.06 ± 0.03	0.12 ± 0.06	0.00 ± 0.00	0.01 ± 0.01
NONI	8	0.33 ± 0.13	0.08 ± 0.03	0.29 ± 0.07	0.11 ± 0.04	0.30 ± 0.08	0.13 ± 0.04	0.16 ± 0.05
NNNI	9	0.28 ± 0.06	0.21 ± 0.09	0.11 ± 0.06	0.09 ± 0.03	0.20 ± 0.12	0.11 ± 0.06	0.72 ± 0.30
NDNI	10	0.19 ± 0.02	0.21 ± 0.07	0.10 ± 0.03	0.10 ± 0.02	0.02 ± 0.01	0.22 ± 0.03	ND
NDDNI	12	0.05 ± 0.05	0.01 ± 0.15	0.18 ± 0.07	0.03 ± 0.03	0.01 ± 0.04	0.04 ± 0.17	ND
DHβE	NA	0.17 ± 0.05	0.37 ± 0.06	0.10 ± 0.04	0.04 ± 0.02	0.15 ± 0.05	0.04 ± 0.02	0.02 ± 0.01

*DHβE indicates dihydro-β-erythroidine; NMNI, *N*-methylnicotinium iodide; NENI, *N*-ethylnicotinium iodide; NPNI, *N*-*n*-propylnicotinium iodide; NnBNI, *N*-*n*-butylnicotinium iodide; NHxNI, *N*-*n*-hexylnicotinium iodide; NHpNI, *N*-*n*-heptylnicotinium iodide; NONI, *N*-*n*-octylnicotinium iodide; NNNI, *N*-*n*-nonylnicotinium iodide; NDNI, *N*-*n*-decylnicotinium iodide; NDDNI, *N*-*n*-dodecylnicotinium iodide; ND, not determined; and NA, not applicable. Data represent the mean ± SEM of the mean of n = 4 to 6 independent observations at each concentration of analog or DHβE. NDNI and NDDNI evoked $^{86}Rb^+$ efflux from thalamic synaptosomes, showing intrinsic activity at 100 μmol/L; however, since efflux did not return to basal levels following analog exposure, total $^{86}Rb^+$ efflux values could not be calculated, therefore these data are not included in the Table.

Inhibition profiles for $C_{9\text{-}12}$ analogs and DHβE, exhibiting IC_{50} values in the nmol/L range, are shown in Figure 3 (top panel). Inhibition profiles for $C_{1\text{-}8}$ analogs, exhibiting IC_{50} values in the μmol/L range, are shown in Figure 3 (bottom panel). The C_{10} analog (NDNI), C_{12} analog (NDDNI), and DHβE were equipotent and completely inhibited the effect of NIC (Figure 3, top panel). The C_9 analog (NNNI) produced a maximal 60% inhibition of the NIC response at a concentration of 100 nmol/L. Table 2 provides IC_{50} values determined for each analog and for DHβE. Furthermore, neither the high nor low affinity components of inhibition of NIC-evoked $^{86}Rb^+$ efflux were correlated significantly with *n*-alkyl chain length (data not shown).

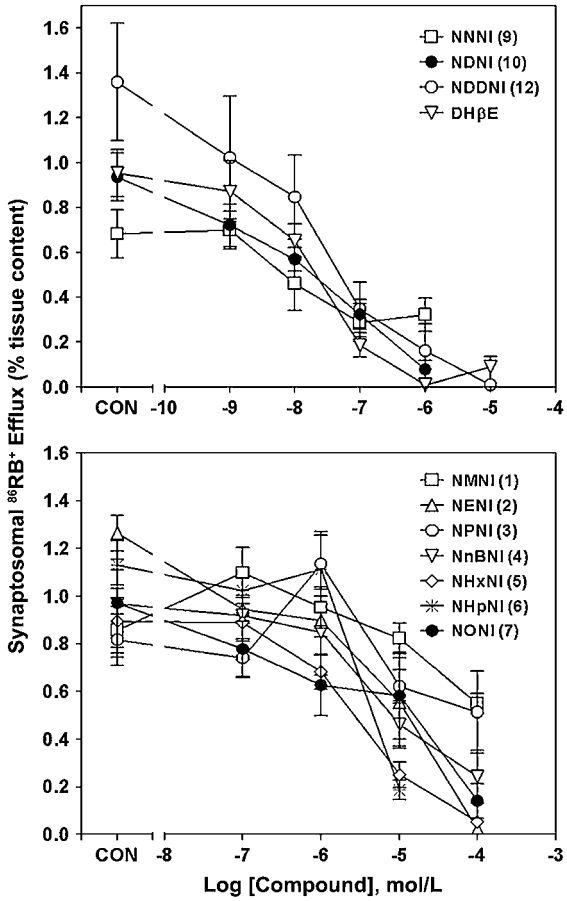

Figure 3. *N-n*-Alkylnicotinium analogs inhibit NIC-evoked $^{86}Rb^+$ efflux from superfused rat thalamic synaptosomes with varying potencies. *N-n*-Alkylnicotinium analog ($C_{1\text{-}12}$) or DHβE was added to the buffer following 120 seconds of superfusion. Superfusion continued for 200 seconds in the presence of analog, DHβE, or buffer before addition of NIC (1 μmol/L) to the buffer. Synaptosomes were superfused in the absence or presence of analog plus NIC for an additional 200 seconds. In each experiment, one synaptosomal aliquot was superfused with 1 μmol/L NIC in the absence of analog or DHβE and served as the NIC control (CON). An additional synaptosomal aliquot was superfused in the absence of either drug and served as the buffer control (data not shown). Data are presented as the mean total $^{86}Rb^+$ efflux 6 SEM as a percentage of tissue $^{86}Rb^+$ content and split into 2 sets based on affinity range. Inhibition profiles for analogs ($C_{9\text{-}12}$) and DHβE, which inhibit NIC-evoked $^{86}Rb^+$ efflux in the low nanomolar range (see Table 2), are shown in the top panel; inhibition profiles for analogs ($C_{1\text{-}8}$), which inhibit NIC-evoked $^{86}Rb^+$ efflux in the low micromolar range (see Table 2), are shown in the bottom panel. Numbers in parentheses in the legends indicate *n*-alkyl chain length. Each data point represents the mean (6 SEM) of 3 to 5 independent observations from individual rats.

DISCUSSION

Structural modification of the NIC molecule has afforded a new class of *N-n*-alkylnicotinium antagonists, which competitively and completely inhibit NIC-evoked [^{3}H]DA overflow from rat striatal slices and [^{3}H]nicotine binding to rat striatal membranes.[22,23] Specifically, NONI potently inhibits its (IC_{50} = 0.62 μmol/L) NIC-evoked [^{3}H]DA overflow but has low affinity (K_i = 20 μmol/L) for [^{3}H]NIC binding sites in striatum. Other compounds in this pharmacological class are potent, competitive inhibitors of high affinity [^{3}H]NIC binding sites, indicating that they interact with α4β2* nAChRs.[22,23] Specifically, NDNI potently inhibits (K_i = 0.09 μmol/L) [^{3}H]NIC binding but does not inhibit NIC-evoked [^{3}H]DA overflow. However, interaction of these analogs with high affinity [^{3}H]NIC binding sites does not indicate if these analogs act as agonists or antagonists at α4β2* nAChR sites. Results from the present study, using a functional assay for high affinity [^{3}H]NIC binding sites in a rat thalamic preparation, demonstrate that *N-n*-alkylnicotinium analogs inhibit NIC-evoked $^{86}Rb^+$ efflux from preloaded synaptosomes and, thus, act as antagonists at these

Table 2. *N-n*-Alkylnicotinium Analog and DHβE Inhibition of NIC (1 μM)-evoked $^{86}Rb^+$ Efflux From Preloaded Rat Thalamic Synaptosomes*

Compound	*n*-Alkyl Chain Length	IC_{50} (μM)	95% CI
NMNI	1	7.16	2.18, 23.6
NENI	2	12.3	6.04, 24.9
NPNI	3	4.63	0.29, 73.7
NnBNI	4	5.6	4.29, 7.31
NHxNI	6	3.07	2.17, 4.34
NHpNI	7	3.83	0.08, 179
NONI	8	6.09	0.80, 46.6
NNNI	9	0.0089	0.0032, 0.025
NDNI	10	0.013	0.0046, 0.040
NDDNI	12	0.016	0.0078, 0.032
DHβE	NA	0.019	0.012, 0.029

*CI indicates confidence interval. All other abbreviations are defined in the first footnote to Table 1. IC_{50} and 95% CI values were derived from curve fits to the means of 4 to 6 independent observations per concentration of analog or DHβE. Data from which these values were derived are presented in Figure 3.

sites. Furthermore, all of the analogs inhibited NIC-evoked $^{86}Rb^+$ efflux at concentrations that did not elicit $^{86}Rb^+$ efflux. However, at a high concentration of 100 μmol/L, $C_{9\text{-}12}$ analogs exhibited robust intrinsic activity, which may be due to nonspecific effects of these analogs or the possibility that these analogs act as partial agonists at α4β2* nAChR sites. Thus, NONI and NDNI have emerged as novel, subtype-selective nAChR antagonists, based on their individual pharmacological profiles (ie, selective inhibition of NIC-evoked DA release and inhibition of NIC-evoked $^{86}Rb^+$ efflux). These analogs should be useful tools for assessing physiological function of specific nAChR subtype in vivo, since they access the brain from the peripheral compartment via the blood-brain barrier choline transporter.[25,26]

Nicotinic agonist-evoked $^{86}Rb^+$ efflux from mouse brain synaptosomes has been shown to be highly correlated with affinity for [^{3}H]NIC binding sites,[9] demonstrating the utility of this assay for determining functional interactions at α4β2* nAChRs. NIC evokes $^{86}Rb^+$ efflux from mouse thalamic synaptosomes with an EC_{50} of 120 to 180 nmol/L.[9,27] The present study using rat thalamic synaptosomes demonstrated an EC_{50} value of 170 nmol/L for NIC, consistent with the previous reports. Two components of NIC-evoked $^{86}Rb^+$ efflux from mouse brain synaptosomes have been defined, based upon sensitivity to DHβE inhibition.[7,8,10] In β2 knockout mice, both DHβE-sensitive and DHβE-resistant components of $^{86}Rb^+$ efflux were eliminated in thalamus and cerebral cortex, demonstrating the requirement for β2 subunits in this receptor-mediated response.[7,8,10] However, no relationship between antagonist affinity for [^{3}H]NIC binding sites and inhibition of NIC-evoked $^{86}Rb^+$ efflux was observed.[9,10,27]

The present study demonstrates that *N*-*n*-Alkylnicotinium analogs inhibit NIC-evoked $^{86}Rb^+$ efflux, demonstrating functional antagonism at α4β2* nAChRs. *N*-*n*-alkylnicotinium analogs produced inhibition of NIC-evoked $^{86}Rb^+$ efflux and could be divided into high ($C_{9\text{-}12}$) and low ($C_{1\text{-}8}$) potency classes. Several possible mechanisms could explain the existence of these 2 distinct potency classes: (1) differential interaction of the analogs with more than one nAChR subtype, (2) interaction with multiple α4β2* isoforms, (3) interaction with alternative subunit stoichiometries of the α4β2* subtype, and (4) interaction with distinct affinity states of the α4β2* nAChR. Coexpression of the α5 subunit with α4 and β2 subunits in cultured cell systems (eg, α4α5β2) has been shown to alter agonist efficacy and potency, as well as receptor desensitization and open channel properties.[28] Furthermore, splice variants of the rat α4 subunit C-terminus have been reported.[29,30] More recently, a single nucleotide polymorphism in the α4 subunit gene has been associated with altered $^{86}Rb^+$ efflux in mouse.[31,32] Alternatively, altered subunit stoichiometries (eg, expression of α4 and β2 subunits in either a 1:9 α:β ratio or a 9:1 ratio) also have been reported to result in nAChRs differentially sensitive to agonist stimulation and antagonist inhibition.[33] Furthermore, differential co-expression of α4 and β2 subunit gene transcripts has been observed in various rat brain regions.[34] On the other hand, distinct affinity states of the α4β2* subtype are consistent with those described by theoretical models.[35-37] Analogs containing *N*-*n*-alkyl substituents of $C_{9\text{-}12}$ chain length (NNNI, NDNI, and NDDNI) may interact preferentially with a high affinity state of α4β2* nAChRs, while $C_{1\text{-}8}$ analogs may interact with a low affinity state. Thus, the high and low potency classes of these analogs may reflect the presence of more than one isoform, stoichiometry, or state of the α4β2* nAChR in rat thalamus.

Of interest, these structurally related *N*-*n*-alkylnicotinium analogs potently (IC_{50} = 0.5-15 nmol/L) inhibited NIC-evoked $^{86}Rb^+$ efflux across a 30-fold range, whereas a significantly greater concentration range (1300-fold) was required to inhibit [^{3}H]NIC binding. At equilibrium, [^{3}H]NIC binding involves the desensitized form of the α4β2* nAChR, generally considered to be the high affinity state.[36] Thus, *n*-alkyl chain length may be a more important factor for analog binding to the high affinity receptor recognition site than for functional inhibition.

However, the current results suggest that an activatable, nondesensitized state of the receptor exhibits significantly higher affinity for *N*-*n*-alkylnicotinium antagonists than does the desensitized state of the receptor. Assuming that both the [^{3}H]NIC binding assay and the inhibition of NIC-evoked $^{86}Rb^+$ efflux assay both define interaction with a common nAChR subtype, it is intriguing that analog-induced inhibition of [^{3}H]NIC binding is a linear function of increasing *n*-alkyl chain length,[23] whereas inhibition of NIC-evoked $^{86}Rb^+$ efflux is not linearly related to *n*-alkyl chain length (current results). Regardless, analog affinity for [^{3}H]NIC binding sites and for inhibition of NIC-evoked $^{86}Rb^+$ efflux varied over a >1000-fold range. Thus, because differences in the overall ranking between affinity for [^{3}H]NIC binding sites (ie, desensitized state) and potency to inhibit NIC-evoked $^{86}Rb^+$ efflux (ie, activatable state) are observed, and since functional interactions cannot be predicted from binding assays alone, the current use of high throughput α4β2* nAChR binding assays to rank drug candidates may not be appropriate. Thus, functional response should be the assay of choice in ranking potential drug candidates to identify leads.

CONCLUSIONS

The present study further extends the characterization of the nAChR properties of a novel class of brain-bioavailable *N*-*n*-alkylnicotinium ligands. The results indicate that $C_{9\text{-}12}$*N*-*n*-alkyl analogs are potent functional inhibitors at α4β2* nAChRs.

The C_{10} analog NDNI exhibits potent and selective antagonism at α4β2* nAChR and may provide a useful tool for elucidating the physiological function of this nAChR subtype, as well as providing a novel therapeutic approach to treating disorders associated with alterations in nAChR function.

ACKNOWLEDGMENTS

This study was supported by National Institutes of Health (NIH) Grants DA00399, DA06043, DA10934, and DA17548. The authors express gratitude to Dr James R. Pauly for technical support in the performance of this research.

REFERENCES

1. Itier V, Bertrand D. Neuronal nicotinic receptors: from protein structure to function. *FEBS Lett*. 2001;504:118-125.

2. Whiting P, Lindstrom J. Pharmacological properties of immunoisolated neuronal nicotinic receptors. *J Neurosci*. 1986;6:3061-3069.

3. Whiting P, Lindstrom J. Purification and characterization of a nicotinic acetylcholine receptor from rat brain. *Proc Natl Acad Sci USA*. 1987;84:595-599.

4. Flores CM, Rogers SW, Pabreza LA, Wolfe BB, Kellar KJ. A subtype of nicotinic cholinergic receptor in brain is composed of alpha 4 and beta 2 subunits and is up-regulated by chronic nicotine treatment. *Mol Pharmacol*. 1992;41:31-37.

5. Picciotto MR, Zoli M, Lena C, et al. Abnormal avoidance learning in mice lacking functional high-affinity nicotine receptor in the brain. *Nature*. 1995;374:65-67.

6. Zoli M, Lena C, Picciotto MR, Changeux J-P. Identification of 4 classes of brain nicotinic receptors using beta2 mutant mice. *J Neurosci*. 1998;18:4461-4472.

7. Marks MJ, Stitzel JA, Grady SR, Picciotto MR, Changeux JP, Collins AC. Nicotinic-agonist stimulated $^{86}Rb^{+}$ efflux and [^{3}H]epibatidine binding of mice differing in β2 genotype. *Neuropharmacology*. 2000;39:2632-2645.

8. Marks MJ, Whiteaker P, Grady SR, Picciotto MR, McIntosh JM, Collins AC. Characterization of [(125)I]epibatidine binding and nicotinic agonist-mediated (86)Rb(+) efflux in interpeduncular nucleus and inferior colliculus of beta2 null mutant mice. *J Neurochem*. 2002;81:1102-1115.

9. Marks MJ, Farnham DA, Grady SR, Collins AC. Nicotinic receptor function determined by stimulation of rubidium efflux from mouse brain synaptosomes. *J Pharmacol Exp Ther*. 1993;264:542-552.

10. Marks MJ, Whiteaker P, Calcaterra J, et al. Two pharmacologically distinct components of nicotinic receptor-mediated rubidium efflux in mouse brain require the beta2 subunit. *J Pharmacol Exp Ther*. 1999;289:1090-1103.

11. Nguyen HN, Rasmussen BA, Perry DC. Binding and functional activity of nicotinic cholinergic receptors in selected rat brain regions are increased following long-term but not short-term nicotine treatment. *J Neurochem*. 2004;90:40-49.

12. Eaton JB, Peng JH, Schroeder KM, et al. Characterization of human α4β2-nicotinic acetylcholine receptors stably and heterologously expressed in native nicotinic receptor-null SH-EP1 human epithelial cells. *Mol Pharmacol*. 2003;64:1283-1294.

13. Karadsheh MS, Shah MS, Tang X, Macdonald RL, Stitzel JA. Functional characterization of mouse α4β2 nicotinic acetylcholine receptors stably expressed in HEK293T cells. *J Neurochem*. 2004;91:1138-1150.

14. Decker MW, Anderson DJ, Brioni JD, et al. Erysodine, a competitive antagonist at neuronal nicotinic acetylcholine receptors. *Eur J Pharmacol*. 1995;280:79-89.

15. Puttfarcken PS, Manelli AM, Arneric SP, Donnelly-Roberts DL. Evidence for nicotinic receptors potentially modulating nociceptive transmission at the level of the primary sensory neuron: studies with F11 cells. *J Neurochem*. 1997;69:930-938.

16. Xiao Y, Meyer EL, Thompson JM, Surin A, Wroblewski J, Kellar KJ. Rat alpha3/beta4 subtype of neuronal nicotinic acetylcholine receptor stably expressed in a transfected cell line: pharmacology of ligand binding and function. *Mol Pharmacol*. 1998;54:322-333.

17. Hernandez SC, Bertolino M, Xiao Y, Pringle KE, Caruso FS, Kellar KJ. Dextromethorphan and its metabolite dextrorphan block α3β4 neuronal nicotinic receptors. *J Pharmacol Exp Ther*. 2000;293:962-967.

18. Lukas R, Fryer J, Eaton J, Gentry C. Some methods for studies of nicotinic acetylcholine receptor pharmacology. In: Levin ED, ed. *Nicotinic Receptors and the Nervous System.* Boca Raton, FL: CRC Press; 2002:3-27.

19. Crooks PA, Ravard A, Wilkins LH, Teng L-H, Buxton ST, Dwoskin LP. Inhibition of nicotine-evoked [^{3}H]dopamine release by pyridine *N*-substituted nicotine analogues: a new class of nicotinic antagonist. *Drug Dev Res*. 1995;36:91-102.

20. Dwoskin LP, Xu R, Ayers JT, Crooks PA. Recent developments in neuronal nicotinic acetylcholine receptor antagonists. *Curr Opin Ther Patents*.. 2000;10:1561-1581.

21. Dwoskin LP, Crooks PA. Competitive neuronal nicotinic receptor antagonists: a new direction for drug discovery. *J Pharmacol Exp Ther*. 2001;298:395-402.

22. Wilkins LH, Haubner A, Ayers JT, Crooks PA, Dwoskin LP. *N-n*-Alkylnicotinium analogs, a novel class of nicotinic receptor antagonist: inhibition of S-(-)-nicotine-evoked [^{3}H]dopamine overflow from superfused rat striatal slices. *J Pharmacol Exp Ther*. 2002;301:1088-1096.

23. Wilkins LH, Grinevich VP, Ayers JT, Crooks PA, Dwoskin LP. *N-n*-Alkylnicotinium analogs, a novel class of nicotinic receptor antagonists: interaction with α4β2* and α7* neuronal nicotinic receptors. *J Pharmacol Exp Ther*. 2003;304:400-410.

24. Xu R, Dwoskin LP, Grinevich V, Sumithran SP, Crooks PA. Synthesis and evaluation of conformationally restricted pyridine *N*-alkylated nicotine analogs as nicotinic acetylcholine receptor antagonists. *Drug Dev Res*. 2002;55:173-186.

25. Allen DD, Lockman PR, Roder KE, Dwoskin LP, Crooks PA. Active transport of high affinity choline and nicotine analogs into the central nervous system by the blood-brain barrier choline transporter. *J Pharmacol Exp Ther*. 2003;304:1268-1274.

26. Crooks PA, Ayers JT, Xu R, et al. Development of subtype selective ligands as antagonists at nicotinic receptors mediating nicotine-evoked dopamine release. *Bioorg Med Chem Lett*. 2004;14:1869-1874.

27. Marks MJ, Robinson SF, Collins AC. Nicotinic agonists differ in activation and desensitization of $^{86}Rb^{+}$ efflux from mouse thalamic synaptosomes. *J Pharmacol Exp Ther*. 1996;277:1383-1396.

28. Ramirez-Latorre J, Yu CR, Qu X, Perin F, Karlin A, Role L. Functional contributions of alpha5 subunit to neuronal acetylcholine receptor channels. *Nature*. 1996;380:347-351.

29. Goldman D, Deneris E, Luyten W, Kochhar A, Patrick J, Heinemann S. Members of a nicotinic acetylcholine receptor gene family are expressed in different regions of the mammalian central nervous system. *Cell*. 1987;48:965-973.

30. Yu ZJ, Morgan DG, Wecker L. Distribution of 3 nicotinic receptor alpha 4 mRNA transcripts in rat brain: selective regulation by nicotine administration. *J Neurochem*. 1996;66:1326-1329.

31. Stitzel JA, Dobelis P, Jimenez M, Collins AC. Long sleep and short sleep mice differ in nicotine-stimulated $^{86}Rb^{+}$ efflux and α4 nicotinic receptor subunit cDNA sequence. *Pharmacogenetics*. 2001;11:331-339.

32. Dobelis P, Marks MJ, Whiteaker P, Balogh SA, Collins AC, Stitzel JA. A polymorphism in the mouse neuronal α4 nicotinic receptor subunit results in an alteration in receptor function. *Mol Pharmacol*. 2002;62:334-342.

33. Zwart R, Vijverberg HP. Four pharmacologically distinct subtypes of α4β2 nicotinic acetylcholine receptor expressed in *Xenopus laevis* oocytes. *Mol Pharmacol*. 1998;54:1124-1131.

34. Liu C, Nordberg A, Zhang X. Differential co-expression of nicotinic acetylcholine receptor alpha 4 and beta 2 subunit genes in various regions of rat brain. *Neuroreport*. 1996;7:1645-1649.

35. Katz B, Thesleff S. A study of the "desensitization" produced by acetylcholine at the motor end-plate. *J Physiol*. 1957;138:63-80.

36. Edelstein SJ, Schaad O, Henry E, Bertrand D, Changeux JP. A kinetic mechanism for nicotinic acetylcholine receptors based on multiple allosteric transitions. *Biol Cybern*. 1996;75:361-379.

37. Karlin A. Emerging structure of the nicotinic acetylcholine receptors. *Nat Rev Neurosci*. 2002;3:102-114.